Benchmarking nuclear models of FLUKA and GEANT4 for carbon ion therapy



2010 Phys. Med. Biol. 55 5833

(http://iopscience.iop.org/0031-9155/55/19/014)

Phys. Med. Biol. **55** (2010) 5833–5847 doi:10.1088/0031-9155/55/19/014

# Benchmarking nuclear models of FLUKA and GEANT4 for carbon ion therapy

**T T Böhlen[1,2], F Cerutti[1], M Dosanjh[1], A Ferrari[1], I Gudowska[2], A Mairani[3] and J M Quesada[4]**

[1] European Organization for Nuclear Research CERN, CH-1211, Geneva 23, Switzerland
[2] Medical Radiation Physics, Karolinska Institutet and Stockholm University, Box 260 S-171 76 Stockholm, Sweden
[3] INFN Milan, Via Celoria 16, 20133 Milan, Italy
[4] Departamento de Física Atómica, Molecular y Nuclear, Universidad de Sevilla, Spain

E-mail: Till.Tobias.Boehlen@cern.ch

Received 16 April 2010, in final form 19 August 2010
Published 16 September 2010
Online at stacks.iop.org/PMB/55/5833

**Abstract**

As carbon ions, at therapeutic energies, penetrate tissue, they undergo inelastic nuclear reactions and give rise to significant yields of secondary fragment fluences. Therefore, an accurate prediction of these fluences resulting from the primary carbon interactions is necessary in the patient's body in order to precisely simulate the spatial dose distribution and the resulting biological effect. In this paper, the performance of nuclear fragmentation models of the Monte Carlo transport codes, FLUKA and GEANT4, in tissue-like media and for an energy regime relevant for therapeutic carbon ions is investigated. The ability of these Monte Carlo codes to reproduce experimental data of charge-changing cross sections and integral and differential yields of secondary charged fragments is evaluated. For the fragment yields, the main focus is on the consideration of experimental approximations and uncertainties such as the energy measurement by time-of-flight. For GEANT4, the hadronic models G4BinaryLightIonReaction and G4QMD are benchmarked together with some recently enhanced de-excitation models. For non-differential quantities, discrepancies of some tens of percent are found for both codes. For differential quantities, even larger deviations are found. Implications of these findings for the therapeutic use of carbon ions are discussed.

(Some figures in this article are in colour only in the electronic version)

## 1. Introduction

Monte Carlo particle transport codes are valuable tools to predict radiation fields of ions in tissues and are used in hadron therapy for the simulation of ion transport and nuclear

  

interactions since they are able to complement and bridge shortcomings of frequently used analytical codes. Several Monte Carlo codes such as FLUKA (Battistoni *et al* 2007, Fassò *et al* 2005), GEANT4 (Agostinelli *et al* 2003, Allison *et al* 2006), MCNPX (Hughes *et al* 1997, LANL 2002), SHIELD/SHIELD-HIT (Dementyev and Sobolevsky 1999, Gudowska *et al* 2004) and PHITS (Niita *et al* 2006) are utilized to calculate fluences and dose distributions in patients or patient-like geometries for proton and/or ion beams. Even though these codes are generally not used for treatment planning optimization as they are currently too time consuming, they are prominent candidates for dose verification of analytical treatment planning codes and their models can be used to complement experimental data and generate systematically data of physical quantities as input for treatment planning codes (Mairani *et al* 2008, Paganetti *et al* 2008, Parodi *et al* 2009, Peterson *et al* 2009).

The radiation field created by therapeutic heavy charged ion beams contains, unlike protons, a large fraction of fragments which significantly contributes to particle fluences and the actual delivered dose. The dose fraction delivered by fragments in the region before the Bragg peak is estimated to be about 20% for a 290 MeV/n carbon beam impacting on PMMA (experiment, counting fragments other than carbon isotopes) (Matsufuji *et al* 2003) and about 40% for a 400 MeV/u carbon beam impacting on water (calculations) (Kempe *et al* 2007). There are two main interests in the accurate modelling of these secondary particle fluences and secondary doses in clinical ion beams. Compared to the radiation field of the primary ions, secondary fragments lead to an altered spatial dose distribution due to differing ranges and angular distributions of the fragments and to a modification of the linear-energy transfer (LET) spectra which results in a difference of biological effectiveness for the same delivered dose. Consequently, an accurate knowledge of ion beam fragmentation is important for a precise description of biological effects inside and outside the treatment volume. Secondly, the precise prediction of nuclear particle interactions and resulting residual nuclei distributions are needed for imaging techniques which aim at *in vivo* dose monitoring. Techniques which are currently being investigated include positron emission tomography (PET) (e.g. Litzenberg *et al* 1999, Priegnitz *et al* 2008) and prompt $\gamma$-ray imaging (e.g. Polf *et al* (2009) and Styczynski *et al* (2009)).

Several recent studies have reported comparisons of nuclear Monte Carlo models of FLUKA (Mairani 2007, Sommerer *et al* 2006) and GEANT4 (Pshenichnov *et al* 2006, 2010) for carbon ion therapy. They provide evidence that the agreement between predictions of nuclear reaction models and experimental data is encouraging but that there is ample room for improvement. However, the extent of the published comparisons is not comprehensive, which is partly due to the few available experimental data and their limited precision.

This work reports a benchmark of the current performance of nuclear reaction models of FLUKA and GEANT4 under identical conditions, and for target-projectile combinations and energies relevant for carbon ion therapy. It compares experimental data of charge-changing cross-sections and fragmentation yields differential in energy and angle. For the fragment yields, the main focus is on a precise consideration of experimental conditions, including uncertainties and approximations of the measurements. For GEANT4, there is a variety of available hadronic models which have to be combined adequately to describe the initial interaction stage and the following pre-equilibrium and equilibrium de-excitation stage. Some of these models have recently undergone major improvements and corrections. The presented comparison of simulations to experimental data provides guidance for adequate choices of the GEANT4 physics models for hadron therapy.

## 2. Methods

FLUKA and GEANT4 are multi-purpose Monte Carlo particle transport codes which allow simulation of the passage of primary ions and the produced secondary particles through matter. They provide interaction models for all electromagnetic and nuclear processes relevant for the transport of therapeutic ion beams. To allow for an objective evaluation of the performance of the physics models implemented in FLUKA and GEANT4, the same simulation approach was pursued for all comparisons, using equal initial beam conditions, geometries and material characteristics. In addition, post processing and analysis of the simulation data were done with the same tools.

### *2.1. FLUKA configuration and code description*

For the presented simulations, the configuration recommended for hadron therapy ('HADROTHErapy') was chosen. This option uses delta-ray production and transport cuts of 100 keV. Neutrons were tracked down to thermal energies. Electromagnetic physics was described within the EMF package which accounts for energy loss, straggling and multiple Coulomb scattering of charged particles. For ion projectile energies from 5 GeV/n down to 100 MeV/n, a relativistic quantum molecular dynamics (rQMD) model (Andersen *et al* 2004) was employed as a hadronic event generator. For lower energies, a model based on the Boltzmann master equation (BME) theory (Cerutti *et al* 2006) was used to describe hadronic interactions. Total nuclear reaction cross-sections were calculated based on an empirically modified version of the Tripathi parametrization for nucleus–nucleus interactions (Andersen *et al* 2004, Tripathi *et al* 1996, 1997b, 1999). De-excitation of the excited fragments was processed with the FLUKA evaporation/fission/fragmentation module. Hadron–nucleus interactions were described by the PEANUT model (Ferrari and Sala 1998, Battistoni *et al* 2006) which includes an intra-nuclear cascade stage followed by a pre-equilibrium stage, and then equilibrium particle emission. Simulations were done with the FLUKA version 2008.3.

### *2.2. GEANT4 configuration and code description*

Electromagnetic interactions were described with a set of models included in the 'electromagnetic standard package option 3'. They account for energy loss, straggling and multiple Coulomb scattering of charged particles. Delta-ray production and particle transport cuts were set to 1 mm in water (equivalent to 350 keV for electrons and 2.9 keV for photons). Hadron–nucleus and nucleus–nucleus interactions and the subsequent pre-equilibrium and de-excitation stages can be described by a variety of GEANT4 models. The GEANT4 physics list QGSP_BIC_HP including the G4BinaryLightIonReaction (Geant4 2009), also called Binary Cascade light ion (BIC LI), is currently the recommended configuration of hadronic physics settings for hadron therapy and was used as standard configuration. In this configuration, hadronic nucleon–nucleus interactions are described by the Binary Cascade (BIC) model (Folger *et al* 2004). The BIC LI model, as an extension of the BIC model to ions, is valid from approximately 80 MeV/n to 10 GeV/n. After the initial interaction stage, highly excited fragment remnants were processed via a pre-compound stage. The G4QMD (Koi 2008) was used as an alternative model to BIC LI to handle ion–ion interactions. It is an integration of the JQMD code (Niita *et al* 1995, 1999) as a native GEANT4 hadronic model, including the GEANT4 scattering and decay library and some additional developments. Compared to the rQMD model used in FLUKA, which is based on an approach using Poincaré-invariant Hamilton dynamics, the JQMD is not fully Lorentz invariant. Total nucleus–nucleus

reaction cross-sections were derived by Tripathi, Tripathi Light (Tripathi *et al* 1996, 1997a, 1999, 1997b), and Shen (Shen *et al* 1989) parametrizations which come from empirical and parametrized formula based on theoretical models. They cover interaction energies from 10 MeV/n to 10 GeV/n. The de-excitation of fragments was described with several models. Evaporation from excited nuclei was handled by default by the Weisskopf–Erwing model (with emission channels $Z \leqslant 2$, $A \leqslant 4$) together with fission and $\gamma$-de-excitation (Geant4 2009). Simulations were done including the more recently integrated models and model options: Fermi Break-Up (for light nuclei $Z \leqslant 8$, $A \leqslant 16$), Statistical Multifragmentation (for excitation energies exceeding 3 MeV/n) and Generalized Evaporation Model (for channels $2 < Z \leqslant 12$, $4 < A \leqslant 28$, excluding channels for light nuclei) (Geant4 2009). All these models have undergone several significant improvements and debugging recently. It is noteworthy that the G4RadioactiveDecay had to be switched on for simulations in order to decay highly unstable fragments produced as remnants of hadronic interactions, such as hydrogen with $A = 5$. Simulations were done with version 9.3.

## 3. Comparison of charge-changing cross-sections

The total and partial charge-changing cross-sections are basic quantities characterizing ion beam reactions in matter. The total charge-changing cross-section is defined as

$$\sigma_{\mathrm{tcc}} = \sigma_{\mathrm{tot}} - \sigma_{\mathrm{el}} - \sigma_{\mathrm{nr}}, \tag{1}$$

where $\sigma_{\mathrm{tot}}$ is the total cross-section, $\sigma_{\mathrm{el}}$ is the elastic cross-section and $\sigma_{\mathrm{nr}}$ is the neutron-only removal cross-section. Partial charge-changing cross-sections $\sigma_{\mathrm{pcc},\Delta Z}$ measure reactions in which a number of protons $\Delta Z$ are removed from the initial fragment with charge $Z_0$ to form a fragment with charge $Z_0 - \Delta Z$. The performance of FLUKA and GEANT4 in predicting charge-changing interactions of carbon ions in water and polycarbonate ($C_{16}H_{14}O_3$) was evaluated by comparing with experimental data mostly from Toshito *et al* (2007) and some other measurements (Golovchenko *et al* 2002, Schall *et al* 1996). These measurements provide data for the total charge-changing cross-sections and partial charge-changing cross-sections for production of lithium, beryllium and boron fragments at energies between 100 to 500 MeV/n. In the experimental data from Toshito *et al*, only secondary particles which have an energy and range sufficiently large to be registered by the experimental devices as a track were counted, i.e. their ranges must be at least in the order of 1–2 mm. Conditions for the other data were similar. For the measurements by Golovchenko *et al*, tracks on the upper and bottom surface of each CR-39 detector sheet (thickness $\sim 600\ \mu$m) were matched to allow exclusion of unwanted events like target-like fragments and bubbles. For the measurements of total charge-changing cross-sections by Schall *et al*, target-like carbon fragments leaving the target were stopped in the air after the target or in the ionization chamber used in coincidence with a plastic-scintillator paddle for $Z$-identification or did not have sufficient energy to produce a signal in both detectors. Consequently, target-like fragments, which have at given projectile energies typical ranges of some microns, were not detected.

Total and partial charge-changing cross-sections were determined with FLUKA and GEANT4 by reduced simulation codes only considering hadronic interactions. Both of these stripped code versions force inelastic interactions for projectile-target combinations at an initial kinetic energy of interest. The FLUKA code utilized the hadronic event generators (rQMD and BME) and subsequent pre-compound and de-excitation models for computing the residuals of the interaction. Similarly, the GEANT4 code was utilized either with the G4QMD or the BIC LI model together with models for the subsequent de-excitation phase. Resulting quantities

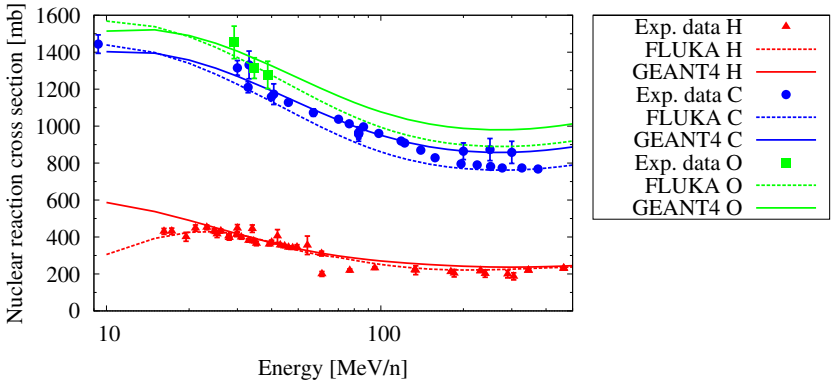


**Figure 1.** Total nuclear reaction cross sections for carbon ions interacting with hydrogen, carbon and oxygen are shown as predicted by FLUKA and GEANT4 together with experimental data (Fang *et al* 2000, Kox *et al* 1984, 1987; Sihver *et al* 1993, Takechi *et al* 2009, Zhang *et al* 2002).

for the different reaction channels were then normalized to the total reaction cross-sections $\sigma_{\mathrm{tr}} = \sigma_{\mathrm{tot}} - \sigma_{\mathrm{el}}$ employed by the code.

### *3.1. Results and discussion*

Figure 1 shows total reaction cross-sections for carbon ions interacting with hydrogen, carbon and oxygen together with experimental data (Fang *et al* 2000, Kox *et al* 1984, 1987, Sihver *et al* 1993, Takechi *et al* 2009, Zhang *et al* 2002). GEANT4 used the Tripathi cross-section parametrization for C–C and C–O interactions and the Tripathi Light cross-section parametrization for C–H interactions. For carbon and oxygen targets, GEANT4 predicts cross-sections which are for energies above 100 MeV/n about 10% higher than the ones predicted by FLUKA. For hydrogen targets, there are notable differences especially for energies below 20 MeV/n. Due to the Coulomb barrier and the minimum excitation energy of 4.4 MeV for $^{12}$C, one would expect a decrease of this cross-section for low energies.

Charge-changing cross-sections for projectile-like fragments in the simulations were compared with the experimental data. The separation between projectile and target-like fragments was done by splitting in forward- and backward-directed fragments in the centre-of-mass system of the nucleons of the initial interaction partners.

A comparison between experimental data and simulations for carbon ions interacting in water and polycarbonate is shown in figures 2 and 3 for total and partial charge-changing cross-sections, respectively. At higher energies, nuclear cross-sections are mostly determined by the geometrical extensions of projectile and target nuclei, and for energies below 1 GeV/n pion production is negligible. Consequently, also the energy dependence of charge-changing cross-sections calculated with both Monte Carlo codes are nearly constant for energies between 200 and 500 MeV/n. For lower energies a steady rise is observed. For FLUKA simulations of carbon ions on water, the total (figure 2) and partial (figure 3) charge-changing cross-sections for Li agree well within the experimental error. Partial charge-changing cross-sections for B and Be are slightly under-estimated. In addition, the presented cross-sections for carbon on polycarbonate are slightly under-estimated by the simulations, except for the cross-section for Be, which agrees well with the data. GEANT4 simulations using the G4QMD model are of similar precision. GEANT4 simulations using the BIC LI model under-estimate experimental

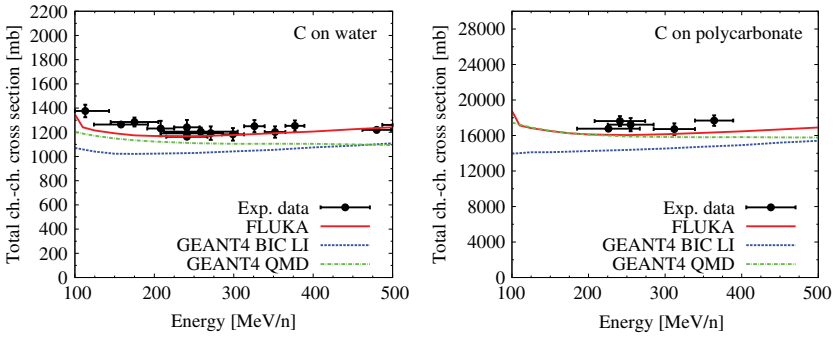


**Figure 2.** Total charge-changing cross-sections for carbon ions interacting with water and polycarbonate ($C_{16}H_{14}O_3$). Vertical error bars indicate the statistical error of the experimental data (Golovchenko *et al* 2002, Schall *et al* 1996, Toshito *et al* 2007).

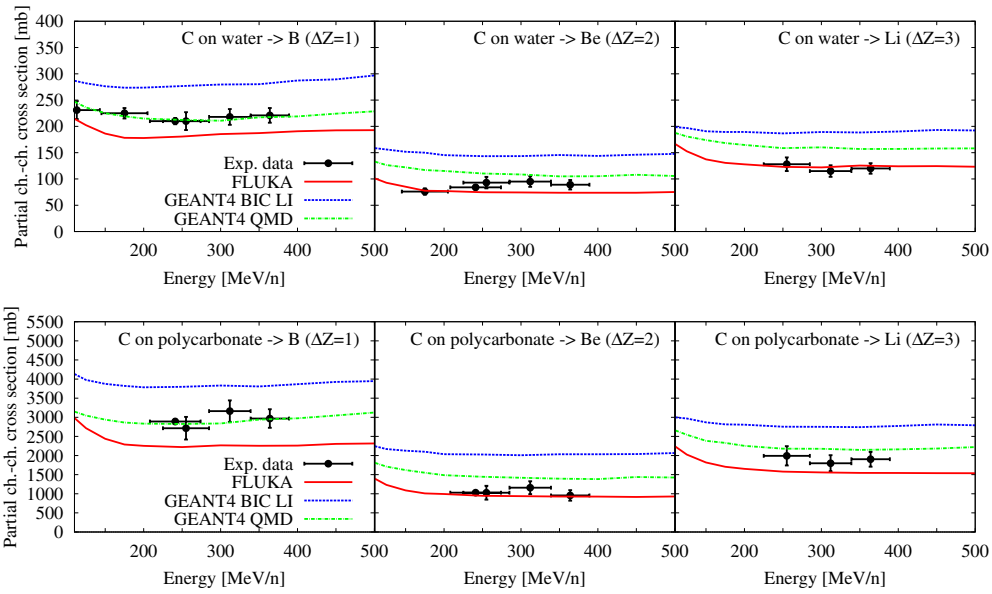


**Figure 3.** Partial charge-changing cross-sections for carbon ions interacting with water and with polycarbonate ($C_{16}H_{14}O_3$) for charge differences of $\Delta Z = 1, 2, 3$. Vertical error bars indicate the statistical error of the experimental data (Golovchenko *et al* 2002, Toshito *et al* 2007).

total charge-changing cross-sections by roughly 20%. Interestingly, this trend is reversed for partial charge-changing cross-sections which are over-estimated by around 50%.

## 4. Comparison of fragment yields at different depths in water

Extensive measurements characterizing the fragmentation of primary $^{12}$C ions at 400 MeV/u in a thick water target were performed by Haettner *et al* (2006) and Haettner (2006). Unlike cross-sections which describe interactions on a single event basis, these data were used for investigating the integral performance of nuclear and atomic models implemented in the Monte Carlo codes for a set-up which represents a strongly simplified approximation to a therapeutic scenario.

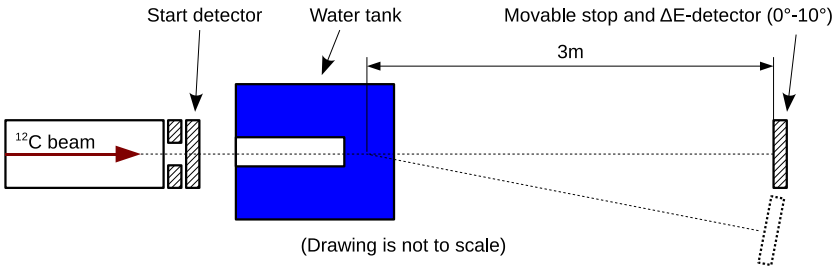


**Figure 4.** Sketch of the experimental set-up for measuring angular distributions and energy distributions by TOF.

Upon target penetration, primary particles are removed by hadronic interactions. Due to fragmentation of the primaries and subsequent de-excitation, fluences of mainly projectile-like nuclei, light clusters and nucleons arise. Target nuclei fragmentation contributes generally with a negligible part to the overall fluences. However, they can be of importance when the focus is set on specific isotope production in those reactions (e.g., for PET imaging). The range of secondary fragments $R_{Z,A}$ with the same energy per nucleon $E$ as the primary projectile is related to the range of the primary projectiles $R_{Z_0,A_0}$ by the ratio of their stopping powers. For the Bethe–Bloch region, it is in good approximation given by

$$R_{Z,A}(E) = \frac{A}{Z^2} \cdot \frac{Z_0^2}{A_0} \cdot R_{Z_0,A_0}(E). \tag{2}$$

Depending on the charge-mass ratio, creation point, and initial energy and angle of the produced fragments, these fragments travel beyond the Bragg peak or are stopped before. With rising primary energy, the contribution of secondary fluences to the delivered dose increases. As a consequence, this test case (primary carbon ions at 400 MeV/u) can be thought of as an upper limit of fragment production for the clinical energy range.

### *4.1. Experimental methods*

Beam fragmentation measurements presented in Haettner *et al* (2006) and Haettner (2006) were done for a 400 MeV/u carbon beam incident on a water target. The experimental details are described elsewhere (Haettner *et al* 2006, Haettner 2006). Below the experimental set-up and techniques are summarized as far as they are of relevance for the comparison with simulations.

The experimental set-up consisted of a triggering detector starting the time measurement, a water target with adjustable thickness and a $\Delta E$-detector which also stopped the time measurement. The arrangement is depicted in figure 4. The $\Delta E$-detector was positioned at a distance $l = 3$ m from the middle of the water target with various angles reaching from 0° to 10°. The time-of-flight (TOF) between the primary carbon ion passing the start detector and an event in the $\Delta E$-detector $t_{\text{meas}}$ was measured. The correlation between TOF and energy loss was used for identification of the different ions (no isotopic separation). This method of particle identification leads to ambiguities in cases where carbon ions and fragments are not well separated as discussed in detail in Haettner (2006). For small angles before the Bragg peak, carbon ions masked the lighter fragments, especially boron and beryllium. Consequently, energy spectra at small angles before the Bragg peak which were chosen for comparison have a data gap. At a depth of 25.8 cm, this gap is at about 70–100 MeV/u, see figure 7.

The energy of the ions was deduced by TOF measurement via the relativistic relation:

$$T = \left( \frac{1}{\sqrt{1-\beta^2}} - 1 \right) \cdot m_0 c^2. \tag{3}$$

Here, $T$ is the kinetic energy of the particle, $\beta$ is the velocity of the particle as a fraction of the speed of light $c$, and $m_0$ is the mass at rest of the particle. For obtaining the velocity of the particle, a twofold approximation was made by the experimental method. It was assumed that the fragmentation of the primary carbon particles takes place in the middle of the target and further that the velocity of the fragment is a constant vector from its point of creation to the detection in the $\Delta E$-detector. This neglects the energy loss of the fragments after their creation.

Under the given assumptions, the velocity of the particle is given by the quotient of the length $l$ and the TOF between the centre of the target and the $\Delta E$-detector $t_{\mathrm{frag}}$. Using the ATIMA code (Geissel and Scheidenberger 1998, Scheidenberger and Geissel 1998), the average time $t_{\mathrm{C}}$ a carbon particle needs for travelling from the start detector to the centre of the water target was calculated. For a measured time $t_{\mathrm{meas}} = t_{\mathrm{C}} + t_{\mathrm{frag}}$, the velocity of the particle was calculated by

$$\beta = \frac{1}{c} \cdot \frac{l}{t_{\mathrm{meas}} - t_{\mathrm{C}}}. \tag{4}$$

Assuming a Gaussian distribution, the time resolution of the detection system was determined to be 0.23 ns (one sigma).

The impact of the discussed experimental uncertainties and approximations on the resulting energy spectra was taken into account by simulations as explained later.

### *4.2. Build-up and angular yields of secondary charged fragments*

The yield of secondary charged fragments was measured at certain depths in the water target. The experimental results are presented as the number of fragments per primary particle versus depth. In this experiment, only fragments with angles smaller than 10° leaving the water target were detected. Due to their wide angular distributions, not all produced hydrogen and helium fragments were detected. For heavier fragments from lithium to boron, the whole angular range was covered and yields are equivalent to the total number of secondaries leaving the target.

Simulations scored particle spectra and angular distributions at different depths in the water volume with small distances so that nearly continuous curves were obtained. Integral fragment yields were obtained excluding particles with angles larger than 10°.

*4.2.1. Results and discussion.* Figure 5 shows the yields of fragments per primary carbon ion versus depth obtained with FLUKA, GEANT4 and from measurements. The yields of fragments increase with depth until the Bragg peak region, where the primaries cease to produce new fragments. After the Bragg peak, the amount of secondaries drops steadily to zero. It can be seen that the relative yield of lithium, beryllium and boron predicted by the three different model options is in agreement with their respective partial charge-changing cross-sections from the former section, as expected.

For H and He ions FLUKA simulations agree within about 10%. There is an under-prediction of Li of maximal about 20% which is not seen in the respective charge-changing cross-section. As the same production cross-sections were employed by the Monte Carlo codes for both simulations, this disagreement might point at uncertainties of the experimental data.

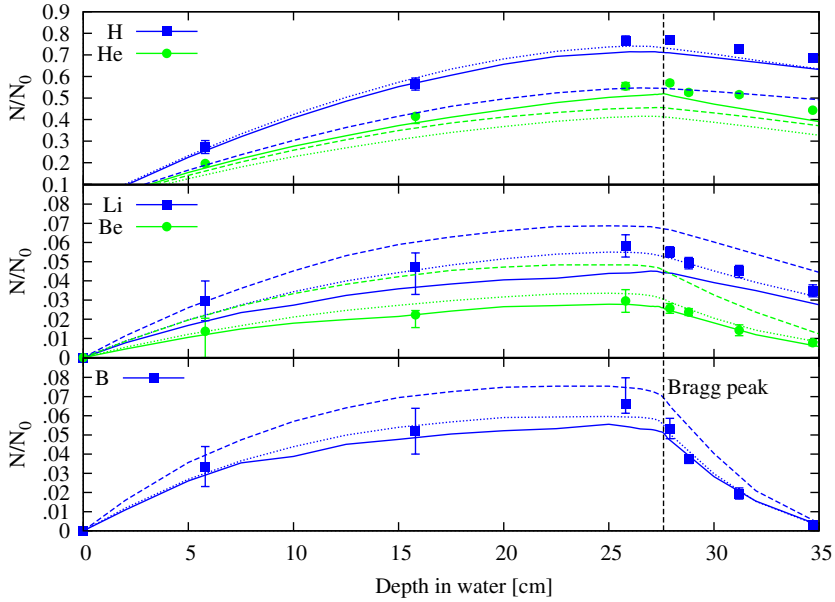


**Figure 5.** Fragment build-up curves in water of a 400 MeV/u carbon beam as a fraction of primary carbon ions $N/N_0$. Experimental data are shown as points (Haettner *et al* 2006). Simulations done for FLUKA (solid) and for GEANT4 using the BIC LI (dashed) and the G4QMD (dotted) model are displayed as lines. The dashed vertical line indicates the position of the Bragg peak.

Heavier fragments are predicted within the experimental error. The GEANT4 simulations employing the G4QMD model reproduce the experimental data rather well and mostly within the experimental precision for all ions, except for He which is under-estimated by maximal about 20–30%. For the GEANT4 BIC LI model, the yields of H and He ions are systematically under-estimated, maximal by about 30%. As already seen from the charge-changing cross-sections, there is an overestimation of Li, Be and B. The sizeable under-prediction of the light fragments H and He by the BIC LI model might also explain the under-estimation of the total charge-changing cross-section despite the fact that partial charge-changing cross-sections of the heavier fragments are over-predicted with respect to measurements. GEANT4 simulations including the Fermi Break-Up and the Statistical Multifragmentation models (as shown in figure 5) yielded a significantly better agreement with the experimental data compared to simulations using only the default de-excitation models. Calculations using the G4QMD model were compared to simulations with the BIC LI model approximately twofold slower. As discussed in Haettner (2006), the production yield of boron ions might be under-estimated in the experiment; this might change somewhat the agreement with the simulations.

Figure 6 shows the normalized angular yields of fragments at a water-equivalent depth of 25.8 cm, just before the Bragg peak. The level of agreement between experimental data and simulation in the proximal end of the Bragg peak and in the region after the Bragg peak is very similar to the presented values at a depth of 25.8 cm. Due to their small solid angle, fragmentation yields of the forward angles contribute only marginally to the integral fragmentation yields (see figure 5). For therapeutic applications, correct predictions of angular fragment distributions are of importance for describing the dose distribution in vicinity and behind the Bragg peak. FLUKA reproduces the overall shape of the angular yields very well. Larger angles are slightly under-estimated and there are some discrepancies in the forward angles, especially for H and Li. For both GEANT4 options, fragmentation yields tend to be

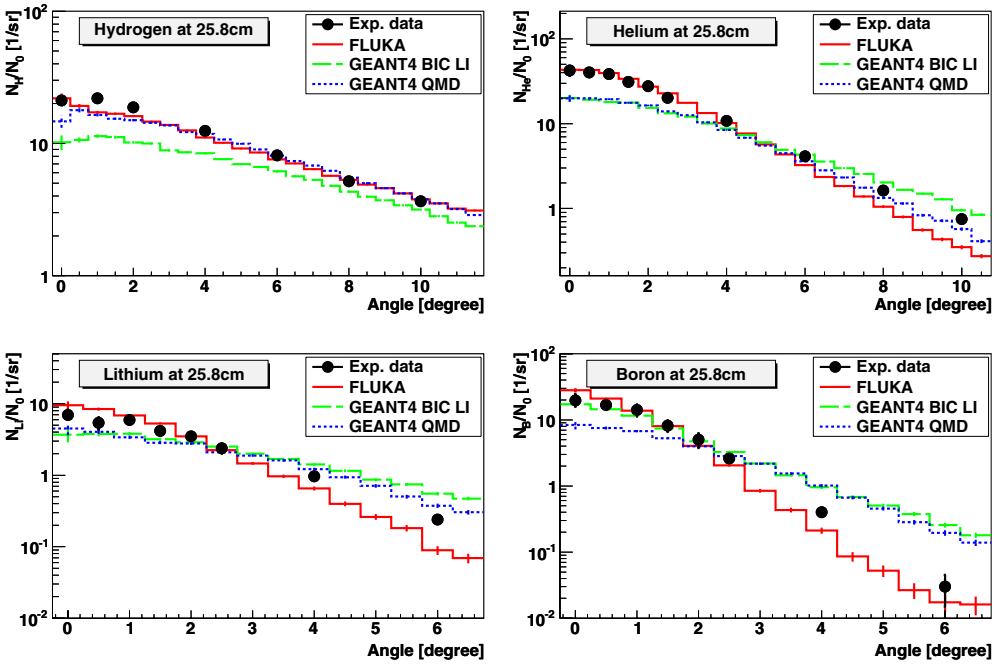


**Figure 6.** Normalized angular yields of H, He, Li and B at a water-equivalent depth of 25.8 cm for a 400 MeV/u carbon beam in water. Yields are expressed as number of ion fragments per steradian per incident primary carbon ion. The vertical error bars of the measurements show an estimation of the error due to the method of particle identification (Haettner 2006). Simulations with FLUKA, GEANT4 BIC LI and GEANT4 G4QMD are shown as lines.

under-estimated for small angles whereas larger angles tend to be over-estimated for fragments heavier than helium. This leads to an integral fragment yield which agrees relatively well with the experimental data as seen in figure 5. As hadron elastic scattering and Coulomb scattering effects for ions heavier than He are generally small, one can assume that the initial angular spectra of produced fragments are not sufficiently forward directed.

### *4.3. Double-differential yields of charged fragments*

The experimental set-up was reproduced with all relevant elements in the beam and original distances. To increase statistics for fragment detection, the rotational symmetry of the set-up was exploited and the $\Delta E$-detector was modelled as eight ring-shaped sections on a semi-sphere with a radius of 3 m. The energy of the particles when entering the $\Delta E$-detector was scored. Deducing the particle energy experimentally via TOF measurements implicates the approximations and uncertainties discussed in section 4.1. Modifications of the energy spectra of the particles due to this experimental method were investigated by reproducing the experimental TOF technique for determining the energy in the simulation. The mean time for the primaries to reach the target centre was calculated and subtracted from the scoring time of the individual particles reaching the $\Delta E$-detector. The energy of the particles was then calculated with (3). The time resolution $\Delta t$ of the detection system was taken into account by introducing a Gaussian distributed random error with the width of the time resolution of the detection system.

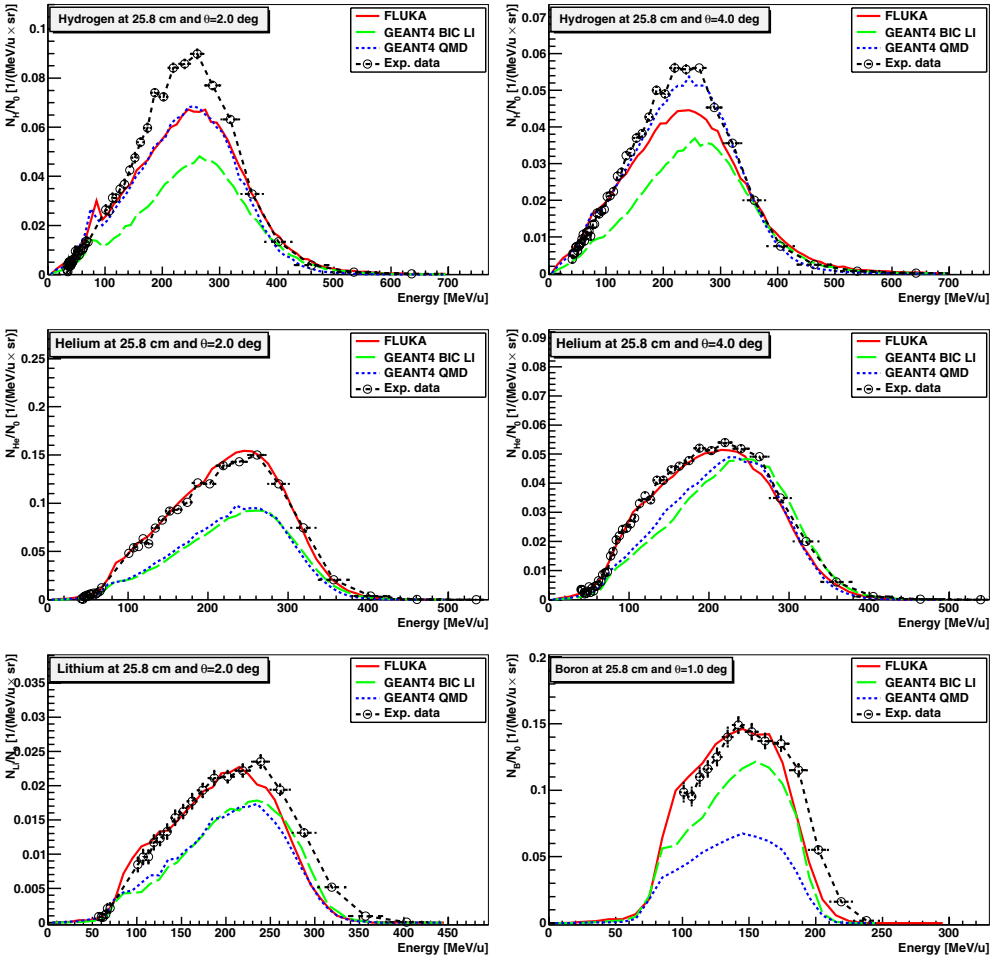


**Figure 7.** Number of ion fragments per steradian per MeV/u normalized to the number of incident particles $N_0$ versus fragment energy are shown as produced by a 400 MeV/u carbon beam in water. Graphs are for a water-equivalent thickness of 25.8 cm and show H, He, Li and B fragments at selected angles. The vertical error bars of the measurements (Haettner 2006) show the statistical error. The horizontal error bars show the time resolution. Simulations with FLUKA, GEANT4 BIC LI and GEANT4 G4QMD are shown. The missing experimental data for 70–100 MeV/u at small angles are due to misidentification of particles (see section 4.1).

*4.3.1. Results and discussion.* Three different target depths were chosen for comparison with simulations: one representing the plateau region (5.9 cm), one before the Bragg peak (25.8 cm) and one after the Bragg peak (31.2 cm). Figure 7 shows the experimental energy spectra of H, He, Li and B at a depth of 25.8 cm and selected angles together with simulations with FLUKA and GEANT4. Graphs shown were selected to correspond to the angles which contribute most to the integral fluences (maximum yield in a fixed $\Delta\theta$ at different azimuthal angles). At a depth of 25.8 cm, this is for heavier fragments from Li to B between $1^\circ$ and $2^\circ$ and for H and He between $2^\circ$ and $4^\circ$.

Below some general aspects of simulated spectra are summarized. Disregarding for a moment the integral yield of fragments at a certain angle, it can be seen that the shape of experimental energy distributions is generally well matched by hadronic models of both codes

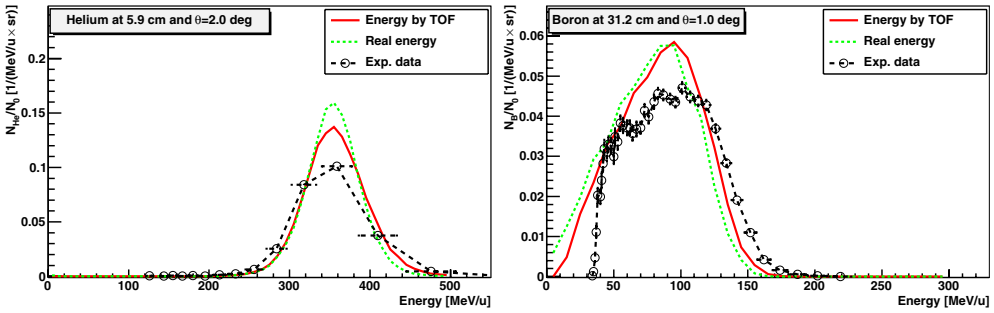


**Figure 8.** Energy spectra of He and B ions at selected angles produced by a 400 MeV/u carbon beam at a water-equivalent thickness of 5.9 cm and 31.2 cm, respectively. Data are shown for measurements (Haettner 2006) and for simulations with FLUKA scoring the particle energy at the detector entrance and calculating the particle energy by TOF measurements taking into account the time resolution of the detection system.

for the different fragments at the selected depths. The spectra of Li, Be (not shown) and B simulations are shifted to slightly lower energies compared to the experimental data.

Systematic uncertainties in the experimental measurements are notable. Measuring the energy of the particles with the TOF technique $E_{\mathrm{TOF}}$ results on average in a slight over-estimation of the real particles' energy $E_{\mathrm{real}}$ in the order of some MeV which was accounted for by the simulation as mentioned before. This over-estimation increases with target thickness as the underlying assumptions of a constant fragment velocity and the fragmentation process occurring in the target centre are less accurate. Further, the agreement between $E_{\mathrm{real}}$ and $E_{\mathrm{TOF}}$ varies for individual particles. This is especially true for light fragments and lower energies. For instance, for hydrogen the standard deviation is about 10–15 MeV. This leads to a broadening of the energy spectra. Lithium, and heavier fragments show no significant spread. At higher energies, additional broadening due to limited time resolution of the detection system occurs, e.g. for 400 MeV/u ions this amounts to about $\Delta E = 23$ MeV/u (one sigma). Figure 8 shows a comparison of different helium and boron spectra resulting from scoring the real particle energies at the detector entrance and from calculating the particle energies by the TOF technique and taking into account a limited time resolution of the detection system. Additional discussion of the uncertainties can be found in Haettner (2006).

Experimental data were taken in two sessions. There is a systematic shift of the energy spectra for the two sessions. Measured carbon energies after 5.9 and 25.8 cm of water match the simulations very well for the first session with an ionization potential for water of 80 eV. For the second session, there is a shift of the carbon energy spectrum towards higher energies of about 40 MeV/u for 5.9 cm and 7 MeV/u for 25.8 cm. The fragment spectra for 25.8 and 31.2 cm were taken during the second session. As mentioned in Haettner (2006), this shift could be due to a possible error in time calibration of the detection system. An offset $t_{\mathrm{err}}$ of 0.2 ns introduced as systematic offset to the simulated TOF of each particle was found to describe more accurately the spectra of the primary carbon ions from the second session. It results in a small shift of heavier fragments at the high energy end of their spectra resulting in a better match. However, this observation does not explain the discrepancies to a full extent.

## 5. Conclusions

The presented analysis demonstrates that current nuclear models of FLUKA and GEANT4 reproduce integral fragment yields with a reasonable accuracy. However, discrepancies in the

order of some tens of percent were found for non-differential quantities for all tested models. They should be improved for their application to carbon ion therapy. The reproduction of forward-directed angles are most problematic for the tested nuclear models. Apart from these very small angles, FLUKA nuclear models describe double-differential spectra rather well. For both investigated GEANT4 models, the yield at small angles is systematically under-estimated while there is a trend to over-estimate larger angles for heavier fragments. For GEANT4, the G4QMD model is preferable over the BIC LI model for the correct prediction of fragment yields. Recent developments of the GEANT4 de-excitation models, specifically the Fermi Break-Up, added substantially to the improved performance. In addition to prior works from Pshenichnov *et al* (2006, 2010), comparisons for GEANT4 are not only made with integral fragment yields but also include yields differential in energy and angle and different choices of the physics configuration, i.e. G4QMD and simultaneous inclusion of de-excitation models, resulting in a better agreement with the experimental data. Compared to the detailed benchmarking of the data from Haettner *et al* (2006) and Haettner (2006) with FLUKA reported by Mairani (2007), a more refined simulation of the experimental data is presented including uncertainties due to energy measurement by TOF.

The relevance of the found discrepancies should be discussed in the context of clinical applications. This is a non-trivial task as a detailed quantitative evaluation of biological dose distributions would require the simulation of a carbon ion treatment field including radiobiological modelling. Still, a strongly simplified calculation for a single Bragg curve (and thus to be interpreted with great care) can estimate the degree of impact on the biological dose one can deduce from found discrepancies and serves as an illustrative example. It is estimated that at maximum around 40% of the dose in the region in front of the Bragg peak is delivered by fragments and that a large fraction of this dose, about 15%, is delivered by protons (Kempe *et al* 2007). Assuming a discrepancy in predicted proton fluences of approximately −30% (as found for GEANT4 BIC LI), and thus an under-estimation of the proton fluences of around 5%, this translates to a difference of 5% in dose delivered by protons, given that the normalized proton energy spectra do not differ significantly. When taking generic values for the relative biologic effectiveness of 1.1, 3.0 and 2.0 for protons, primary carbon ions and all other fragments, respectively, and assuming that the 5% dose which is not delivered by protons is delivered by primary carbon ions instead, one predicts an over-estimation of the biological dose of 4%. For practical purposes with an aimed homogeneous biological dose coverage in the target volume to treat the tumour, this over-estimation by simulations would translate to an under-dosage of the target volume. The dose deposition in the tail region behind the Bragg peak is entirely due to fragments and consequently the biological dose delivered in this region is even more sensitive to changes of contributions from different fragment species. As a consequence of an over-prediction of the large-angle fragment yields which was found for GEANT4, one expects a slightly less confined dose predicted by GEANT4 simulations for a clinical set-up.

It should be emphasized that there is currently a very limited set of experimental fragmentation data with substantial uncertainties. By detailed simulations of the available experiments, more accurate comparisons of experimental data and calculations are expected to be achieved. It was found that a reproduction of the experimental TOF technique by simulation yielded a small but notable improvement for compared energy spectra. In future, extensive and high quality measurements of differential cross-sections and particle yields are needed to improve and validate nuclear interaction models for hadron therapy.

## Acknowledgments

The authors would like to thank G Folger (CERN) and V Ivantchenko (CERN) for discussions on the physics models of GEANT4 and their implementation. Further they thank D Schardt (GSI) for providing measurement data in electronic form. This research project has been supported by a Marie Curie Early Initial Training Network Fellowship of the European Community's Seventh Framework Programme under contract number (PITN-GA-2008-215840-PARTNER).

## References

Agostinelli S, Allison J, Amako K, Apostolakis J and Araujo H 2003 Geant4—a simulation toolkit *Nucl. Instrum. Methods* A **506** 250–303

Allison J *et al* 2006 Geant4 developments and applications *IEEE Trans. Nucl. Sci.* **53** 270–8

Andersen V *et al* 2004 The FLUKA code for space applications: recent developments *Adv. Space Res.* **34** 1302–10

Battistoni G, Cerutti F, Engel R, Fassò A, Ferrari A, Gadioli E, Garzelli M V, Ranft J, Roesler S and Sala P R 2006 Recent developments in the FLUKA nuclear reaction models *Proc. 11th Int. Conf. on Nucl. React. Mech. (Varenna, Italy, 12–16 June)* pp 483–95

Battistoni G *et al* 2007 The FLUKA code: description and benchmarking *Proc. Hadronic Shower Simulation Workshop 2006: AIP Conf. Proc.* vol 896 pp 31–49

Cerutti F, Battistoni G, Capezzali G, Colleoni P, Ferrari A, Gadioli E, Mairani A and Pepe A 2006 Low energy nucleus–nucleus reactions: the BME approach and its interface with FLUKA *Proc. 11th Int. Conf. on Nucl. React. Mech. (Varenna, Italy, 12–16 June)* pp 507–11 Available at http://www.mi.infn.it/∼gadioli/Varenna2006/Proceedings/Cerutti_F.pdf

Dementyev A V and Sobolevsky N M 1999 SHIELD—universal Monte Carlo hadron transport code: scope and applications *Radiat. Meas.* **30** 553–7

Fang D Q *et al* 2000 Measurements of total reaction cross sections for some light nuclei at intermediate energies *Phys. Rev.* C **61** 064311

Fassò A *et al* 2005 FLUKA: a multi-particle transport code *Technical Report* CERN-2005-10, INFN/TC_05/11, SLAC-R-773

Ferrari A and Sala P R 1998 *The Physics of High Energy Reactions* vol 2 (Singapore: World Scientific) pp 424–532

Folger G, Ivanchenko V N and Wellisch J P 2004 The Binary Cascade: nucleon nuclear reactions *Eur. Phys. J.* A **21** 407–17

Geant4 2009 *Geant4 Physics Reference Manual* version 9.3, chapters 26, 29, 30, 31, 32, 33 http://geant4.web.cern.ch/geant4/UserDocumentation/UsersGuides/PhysicsReferenceManual/fo/PhysicsReferenceManual.pdf

Geissel H and Scheidenberger C 1998 Slowing down of relativistic heavy ions and new applications *Nucl. Instrum. Methods* B **136–138** 114–24

Golovchenko A N, Skvarc J, Yasuda N, Giacomelli M, Tretyakova S P, Ilic R, Bimbot R, Toulemonde M and Murakami T 2002 Total charge-changing and partial cross-section measurements in the reactions of ∼110–250 MeV/nucleon 12C in carbon, paraffin, and water *Phys. Rev.* C **66** 014609

Gudowska I, Sobolevsky N, Andreo P, Belkić D and Brahme A 2004 Ion beam transport in tissue-like media using the Monte Carlo code SHIELD-HIT *Phys. Med. Biol.* **49** 1933–58

Haettner E 2006 Experimental study on carbon ion fragmentation in water using GSI therapy beams *Master's Thesis* Kungliga Tekniska Hogskolan Stockholm. Data available at EXFOR: http://www-nds.iaea.org/exfor/exfor.htm

Haettner E, Iwase H and Schardt D 2006 Experimental fragmentation studies with $^{12}$C therapy beams *Radiat. Prot. Dosim.* **122** 485–7

Hughes G, Adams K J, Chadwick M B, Comly J C, Frankle S C, Hendricks J S, Little R C, Prael R E, Waters L S and Young P G Jr 1997 MCNPXTM–The LAHETTM/MCNPTM code merger *Proc. 3rd Workshop on Simulating Accelerator Radiation Environments (SARE 3) (Tsukuba, Japan, 7–9 May): KEK Proceedings (June 1997)* pp 44–51

Kempe J, Gudowska I and Brahme A 2007 Depth absorbed dose and LET distributions of therapeutic 1H, 4He, 7Li, and 12C beams *Med. Phys.* **34** 183–92

Koi T 2008 New native QMD code in Geant4 *IEEE Nuclear Science Symposium Conf. Record. 2008 (NSS '08)*

Kox S, Gamp A, Cherkaoui R, Cole A J, Longequque N, Menet J, Perrin C and Viano J B 1984 Direct Measurements of heavy-ion total reaction cross sections at 30 and 83 MeV/nucleon *Nucl. Phys.* A **420** 162–72

Kox S *et al* 1987 Trends of total reaction cross sections for heavy ion collisions in the intermediate energy range *Nucl. Phys.* C **35** 1678–91

LANL 2002 *MCNPX User's Manual, Version 2.4.0*

Litzenberg D W, Roberts D A, Lee M Y, Pham K, Vander Molen A M, Ronningen R and Becchetti F D 1999 On-line monitoring of radiotherapy beams: experimental results with proton beams *Med. Phys.* **26** 992–1006

Mairani A 2007 Nucleus–nucleus interaction modelling and applications in ion therapy treatment planning *PhD Thesis* University of Pavia

Mairani A, Parodi K, Brons S, Cerutti F, Ferrari A, Gadioli E and Sommerer F 2008 Clinical implementation of full Monte Carlo dose calculation in proton beam therapy *Nucl Sci. Symp. Conf. Record* pp 5612–5

Matsufuji N, Fukumura A, Komori M, Kanai T and Kohno T 2003 Influence of fragment reaction of relativistic heavy charged particles on heavy-ion radiotherapy *Phys. Med. Biol.* **48** 1605–23

Niita K, Chiba S, Maruyama T, Maruyama T, Takada H, Fukahori T, Nakahara Y and Iwamoto A 1995 Analysis of the (N, xN0) reactions by quantum molecular dynamics plus statistical decay model *Phys. Rev.* C **52** 2620–35

Niita K, Chiba S, Maruyama T, Maruyama T, Takada H, Fukahori T, Nakahara Y and Iwamoto A 1999 Development of JQMD (Jaeri Quantum Molecular Dynamics) Code *Nippon Genshiryoku Kenkyujo JAERI, Data, Code 99042*

Niita K, Sato T, Iwase H, Nose H, Nakashima H and Sihver L 2006 PHITS—a particle and heavy ion transport code system *Radiat. Meas.* **41** 1080–90

Paganetti H, Jiang H, Parodi K, Slopsema R and Engelsman M 2008 Clinical implementation of full Monte Carlo dose calculation in proton beam therapy *Phys. Med. Biol.* **53** 4825–53

Parodi K, Brons S, Cerutti F, Ferrari A, Mairani A, Paganetti H and Sommerer F 2009 The FLUKA code for application of Monte Carlo methods to promote high precision ion beam therapy *Proc. 12th Int. Conf. on Nucl. React. Mech. (Varenna, Italy, 15–19 June)* Available at http://cdsweb.cern.ch/record/1238366/files/p509.pdf

Peterson S, Polf J C, Bues M, Ciangaru G, Archambalt L, Beddar S and Smith A R 2009 Clinical implementation of full Monte Carlo dose calculation in proton beam therapy *Phys. Med. Biol.* **54** 3217–29

Polf J C, Peterson S, McCleskey M, Roeder B T, Spiridon A, Beddar S and Trache L 2009 Measurement and calculation of characteristic prompt gamma ray spectra emitted during proton irradiation *Phys. Med. Biol.* **54** N519–27

Priegnitz M, Möckel D, Parodi K, Sommerer F, Fiedler F and Enghardt W 2008 In-beam PET measurement of 7Li3+ irradiation induced beta+-activity *Phys. Med. Biol.* **53** 4443–53

Pshenichnov I, Botvina A, Mishustin I and Greiner W 2010 Nuclear fragmentation reactions in extended media studied with Geant4 toolkit *Nucl. Instrum. Methods* B **268** 604–15

Pshenichnov I, Mishustin I and Greiner W 2006 Distributions of positron-emitting nuclei in proton and carbon-ion therapy studied with GEANT4 *Phys. Med. Biol.* **51** 6099–112

Schall I *et al* 1996 Charge-changing nuclear reactions of relativistic light-ion beams ($5 \leqslant Z \leqslant 10$) passing through thick absorbers *Nucl. Instrum. Methods* B **117** 221–34

Scheidenberger C and Geissel H 1998 Penetration of relativistic heavy ions through matter *Nucl. Instrum. Methods* B **135** 25–34

Shen W Q, Wang B, Feng J, Zhan W L, Zhu Y T and Feng E P 1989 Total reaction cross section for heavy-ion collisions and its relation to the neutron excess degree of freedom *Nucl. Phys.* A **491** 130–46

Sihver L, Tsao C H, Silberberg R, Kanai T and Barghouty A F 1993 Total reaction and partial cross section calculations in proton-nucleus ($Z_t \leqslant 26$) and nucleus–nucleus reactions ($Z_p$ and $Z_t \leqslant 26$) *Phys. Rev.* C **47** 1225–36

Sommerer F, Parodi K, Ferrari A, Poljanc K, Enghardt W and Aiginger H 2006 Investigating the accuracy of the FLUKA code for transport of therapeutic ion beams in matter *Phys. Med. Biol.* **51** 4385–98

Styczynski J, Riley K, Binns P, Bortfeld T and Paganetti H 2009 Can prompt gamma emission during proton therapy provide in situ range verification *Med. Phys.* **36** 2425–6

Takechi M *et al* 2009 Reaction cross sections at intermediate energies and Fermi-motion effect *Phys. Rev.* C **79** 061601

Toshito T *et al* 2007 Measurements of total and partial charge-changing cross sections for 200- to 400-MeV/nucleon $^{12}$C on water and polycarbonate *Phys. Rev.* C **75** 054606

Tripathi R K, Cucinotta F A and Wilson J W 1996 Accurate universal parameterization of absorption cross sections *Nucl. Instrum. Methods* B **117** 347–9

Tripathi R K, Cucinotta F A and Wilson J W 1997a Universal parameterization of absoption cross sections Technical Report NASA Technical Paper 3621, NASA

Tripathi R K, Cucinotta F A and Wilson J W 1999 Accurate universal parameterization of absorption cross-sections III—light systems *Nucl. Instrum. Methods* B **155** 349–56

Tripathi R K, Wilson J W and Cucinotta F A 1997b Accurate universal parameterization of absorption cross sections II—neutron absorption cross sections *Nucl. Instrum. Methods* B **129** 11–5

Zhang H Y *et al* 2002 Measurement of reaction cross section for proton-rich nuclei (A<30) at intermediate energies *Nucl. Phys.* A **707** 303–24